**To link to this article** : DOI: 10.1002/adma.201605745
URL : http://dx.doi.org/10.1002/adma.201605745

# Light Control of Charge Transfer and Excitonic Transitions in a Carbon Nanotube/Porphyrin Hybrid

*Yani Chen, Guy Royal, Emmanuel Flahaut, Saioa Cobo, Vincent Bouchiat, Laëtitia Marty, and Nedjma Bendiab**

**Carbon nanotube–chromophore hybrids are promising building blocks in order to obtain a controlled electro-optical transduction effect at the single nano-object level. In this work, a strong spectral selectivity of the electronic and the phononic response of a chromophore-coated single nanotube transistor is observed for which standard photogating cannot account. This paper investigates how light irradiation strongly modifies the coupling between molecules and nanotube within the hybrid by means of combined Raman diffusion and electron transport measurements. Moreover, a nonconventional Raman enhancement effect is observed when light irradiation is on the absorption range of the grafted molecule. Finally, this paper shows how the dynamics of single electron tunneling in the device at low temperature is strongly modified by molecular photoexcitation. Both effects will be discussed in terms of photoinduced excitons coupled to electronic levels.**

Low-dimensional sp$^2$ carbon nanostructures such as graphene and nanotubes have emerged as ideal platforms for molecular electronics enabling new functional devices such as ultrasensitive molecule detectors, molecular scale logics, and quantum devices.[1] In particular, nanotube ambipolar behavior along with direct band gap allows their use for optoelectronics.[2] However, single wall nanotubes (SWNTs) are sensitive to any nonspecific and slight fluctuation in their environment, which directly alters their optoelectronic properties. Grafting chromophores onto nanotubes is a hybrid route toward specific functions for nanoelectronics. It is of great interest and challenging to reach the limit of hybrids at the single nanotube level. In this limit, the number of active molecules is limited by 1D geometry and a single nano-object can be detected.[3–10] In the particular case of optically active hybrids, zinc(II) metalloporphyrins coating a SWNT network field effect transistor (FET) device was proposed for light harvesting.[11] Recent applications of porphyrins for dye-sensitized solar cells have shown high yield in light energy harvesting.[12] However, only few studies have demonstrated efficient photoinduced charge transfer in nanotubes/porphyrins hybrid systems by using electrochemical methods,[13] photoluminescence excitation experiments,[14] and absorption spectroscopy.[15] These works highlight the importance of energy and/or charge transfer between molecules and nanotubes either in assembly of nanotubes or in isolated nanotubes in solution. Here we investigate how light excitation can be used to tune the signatures of the hybrids related to nanotube/chromophore coupling: the enhancement of the Raman signal from the so-called graphene-enhanced Raman spectroscopy effect (GERS)[16,17] and the onset of single charge trapping with molecular traps.[18] These well-known effects should dramatically depend on light exposure in the case of chromophores, which has not been addressed yet.

To investigate the dependence of electronic and phononic response of a chromophore-coated single nanotube transistor under light irradiation, our approach consists in using complementary Raman spectroscopy and electron transport measurements on the same samples. First, we will discuss how grafting chromophores on a single nanotube transistor induces a visible charge transfer in both phononic and electronic response. Second, we report on a strongly nonconventional vibrational response under light irradiation of the hybrid at different wavelengths. Finally, we will address the possibility to control the dynamics of single charge trapping with light at low temperature. The chromophore used here is a porphyrin moiety metallated with a zinc(II) ion in its center named as zinc(II)-meso-tetraphenylporphyrin (see **Figure 1**a, TPPZn).

Porphyrins provide an extremely versatile synthetic platform for a variety of applications.[19] Their optical properties are very interesting for energy transfer with molecular control[14,20] and for potential applications in optoelectronics.[21] The absorption spectrum of TPPZn in toluene exhibits an intense Soret band at 422 nm and a main Q band at 549 nm (see Figure 1a).[22,23]

Dr. Y. Chen, Dr. V. Bouchiat, Dr. L. Marty, Dr. N. Bendiab
Institut Néel
CNRS
BP 166, Grenoble Cedex 9
38042 Grenoble, France
E-mail: nedjma.bendiab@neel.cnrs.fr

Dr. Y. Chen, Dr. V. Bouchiat, Dr. L. Marty, Dr. N. Bendiab
Institut Néel
Univ. Grenoble Alpes
F-38000 Grenoble, France

Prof. G. Royal, Dr. S. Cobo
Univ. Grenoble Alpes
CNRS, Département Chimie Moléculaire (UMR 5250)
F-38000 Grenoble, France

Dr. E. Flahaut
CIRIMAT, UMR CNRS-UPS-INP No5085
Université Toulouse 3 Paul Sabatier
Bât. CIRIMAT, 118, route de Narbonne
31062 Toulouse Cedex 9, France

**DOI: 10.1002/adma.201605745**

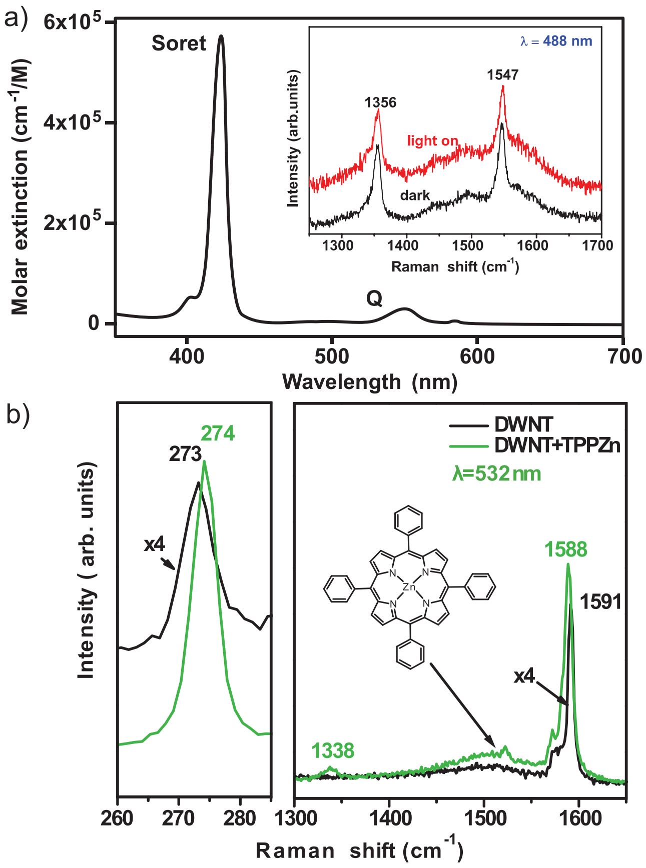


**Figure 1.** a) UV–visible absorption spectrum of TPPZn (inset: Raman spectra of TPPZn powder with (red) and without (black) extra white light illumination. The Raman spectra are measured at excitation wavelength of 488 nm). b) Raman spectra of isolated pristine (black) and hybrid (green) transistor at 532 nm (inset: chemical structure of the zinc(II) metalloporphyrin derivative (TPPZn)).

This zinc-based molecule was demonstrated to provide photogating on nanowires and nanotubes[11,24] and furthermore presents the advantage of being reversibly charged by using light excitation in an easily accessible visible range. The Raman spectrum of TPPZn powder at 532 nm excitation line presents a huge luminescence which does not allow us to measure the Raman fingerprint of the molecule (not shown) whereas the one at 488 nm presents the two main molecular modes at 1356 and 1547 $cm^{-1}$ corresponding to the C—C bond vibration and to combined modes of C—C vibration and C—N vibration[25] (Figure 1b).

This study was conducted on 16 double wall carbon nanotube FETs (CNFETs), which exhibit similar behavior under grafting and light irradiation. First step consists in characterizing the double wall nanotube (DWNT) electronic nature by cross-correlating Raman spectra and gate transfer characteristics. In Figure 1b, one radial breathing like mode (RBLM) and the G Raman modes of a hybrid DWNT transistor are presented. Since resonance conditions were not completely fulfilled for all FETs, we focus, in the following, on a typically resonant transistor for the sake of clarity in the observed effect. In the G band region, a main peak around 1589 $cm^{-1}$ is observed along with a metallic-like Breit–Wigner–Fano shoulder. The G band shape and the position of the RBLM are compatible with an inner semiconducting tube and an outer metallic tube (see Supporting Information for details). After acquiring the Raman spectra and *I–V* curves of the pristine device, a solution of TPPZn in tetrahydrofuran (THF) was drop-casted onto DWNT transistors which were then rinsed with THF and dried under nitrogen. This on chip grafting is necessary to compare the transistor behavior before and after the grafting though it prevents an easy control of the molecules density since the nanotube is a 1D object lying on a substrate. Atomic force microscopy (AFM) (see Supporting Information) shows that molecules tend to cluster onto the nanotube (cluster size of about 30 nm).

At 532 nm, we observe the presence of the TPPZn fingerprint superimposed onto the nanotube one, whereas any signature was hidden by luminescence in the molecule powder at this wavelength. This quenching of TPPZn luminescence by the nanotube at this wavelength allows us to detect the molecular Raman modes, which are also an indication of the effective coupling between these two moieties.[7,26,27] Moreover, after the deposition, the nanotubes modes are enhanced by a factor four to seven in intensity and their frequency are downshifted by 3 $cm^{-1}$ for the G mode (Figure 1b). These signatures indicate a charge transfer between molecules and nanotubes after grafting.[28] Furthermore, such intensity enhancement and luminescence quenching are a signature of chemical enhancement from charge transfer and/or dipolar effect between the nanotube and the molecules.[17,26] Regarding transistor operation at room temperature (see Supporting Information), the hybrid CNFET exhibits a shift corresponding to p-type doping of the field effect characteristics upon molecular deposition which is in agreement with the G band frequency downshift. Moreover, the nanotube hybrid transistor shows a relatively reduced conductance in the off state (1.3 nS), and an on-to-off ratio of 65, in agreement with previous reports of porphyrin-coated SWNT FETs, which was explained as the result of the addition of charged scattering sites distributed randomly along the nanotube.[7] These features are typical of nanotube/molecular hybrids; we will focus in the following on the evolution of these electronic and phononic features under light exposure.

**Figure 2** shows the influence of light illumination on a typical CNFET. We compare the vibrational and electrical responses of this CNFET under light irradiation with wavelength range outside the absorption bands of the molecule (470–480 nm) and with a wavelength in the absorption range of the molecule (550–560 nm). Figure 2a,b shows that the *I–V* curve is not significantly changed under illumination at 475 nm whereas a shift about +1.3 V is observed for an illumination at 555 nm. When shining green light over the sample, 13 FETs (81%) show positive shifts of the threshold voltage (with a mean shift of +3 V) corresponding to holes transfer from the molecule to the nanotube under light illumination. Actually, TPPZn molecules turn negatively charged upon irradiation and act as an additional gate onto the nanotube.[22]

This spectral selectivity is also observed on the phononic response. Actually, we record Raman spectra of the devices under white light illumination for both 488 and 532 nm Raman laser excitations (**Figure 3**). At 532 nm excitation line, only a global enhancement is observed (Figure 2a) whereas at 488 nm, a nonconventional Raman behavior is observed. First,

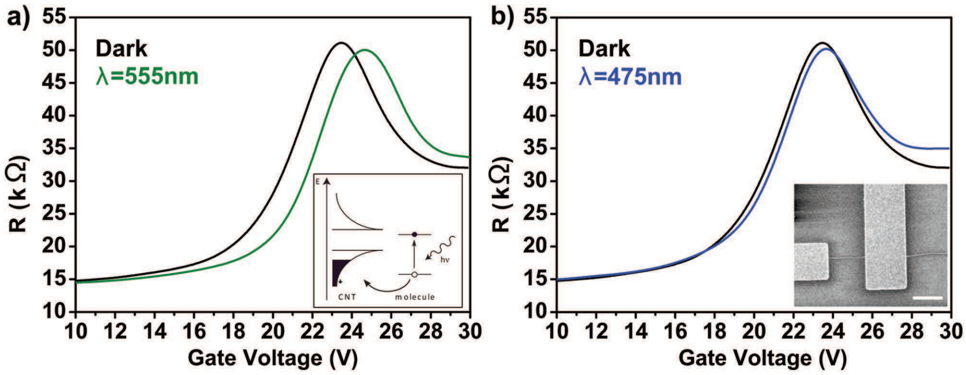


**Figure 2.** Light effect on hybrid CNFET. a) Transfer characteristics at room temperature in dark (black) and under 2 mW laser excitation at a) 475 nm (green) and b) 555 nm (blue) (inset: left, sketch of the molecular optical grafting effect; right, SEM image of an isolated DWNT transistor, scale bar is 1 μm).

at 532 nm, a slight reversible frequency upshift of the G band components is measured from the dark to the light on state (see Supporting Information for the fitting details), allowing us to conclude that only a small charge transfer occurs. Another general feature that appears under light illumination is the broadening of the $G^-$ peak and an increase of the background. These effects are compatible with a weak charge transfer and a partial luminescence from molecules, respectively.

Second, at 488 nm, the enhancement of the G modes is far different from the 532 nm case. The G mode region exhibits dramatic changes: under light exposure only, two large peaks turn out to be visible, one of them matching the dark state G mode with an upshift of 1 $cm^{-1}$ and an intensity twice higher, whereas the most intense one at 1587 $cm^{-1}$ was barely visible in the dark state. When the light is turned off, the new observed intense peak vanishes, while the other mode remains, still shifted by 1 $cm^{-1}$ and reduced in intensity. Different explanations can be proposed for such a photoinduced signature. The first one is that the nanotube is not fully covered with the molecules, thus some parts of it could sense the optical gating from the molecules whereas some remain unchanged. This would lead to a spectrum featuring superimposed peaks from the two portions, coupled and not to the molecules. In such case we would expect to observe superimposed features also in the dark state which is not the case. Moreover, light excitation brings the molecules in a new redox state which is stable for a few hours at room temperature. Such a state can transfer the photogenerated charges to the nanotube as visible by the shift of the G mode. This shift is compatible with surface charges on the nanotube induced by the molecules but it cannot account for the rise of an enhanced peak when light is on.

Actually, under light irradiation, the Soret and Q states of the porphyrin are populated so that energy is transferred from these molecular states to the nanotube excitonic state as already observed in SWNT photoluminescence experiments.[29] Excitonic states can have a major influence on the Raman intensity: if the Raman diffusion process involves a transition between a vibronic state of the nanotube that is close to an excitonic one, the coupling between these states allows the enhancement of the Raman cross section as described by Islam et al.[30] They observed such an enhancement for a phonon mode of CdSe quantum dots coupled to pyridine molecules where the laser excitation energy is in resonance with a charge transfer state and an excitonic state of the hybrid. In our case, we thus attribute the enhancement of one intrinsic mode of the nanotube G band to a Raman process promoted by charge transfer resonance and an excitonic resonance in our hybrid device. Since the two optical phonons $G^+$ and $G^-$ present different symmetries, they will be enhanced differently depending on the dipolar influence of the excitons in the system. Regarding

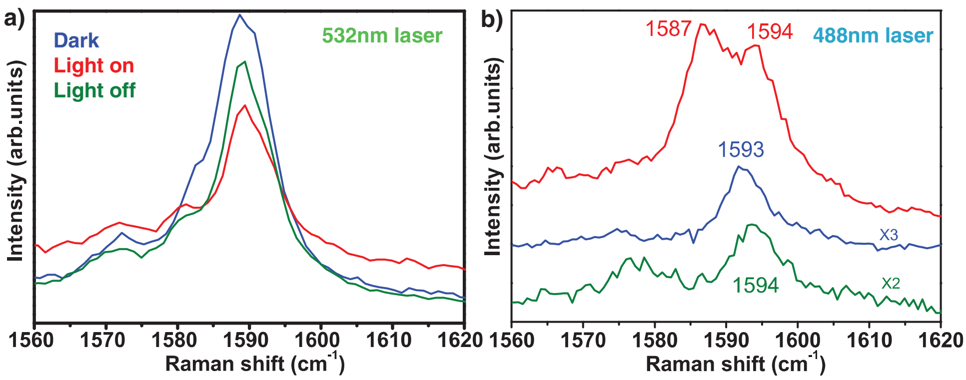


**Figure 3.** Raman spectra of DWNT/TPPZn under white light illumination measured at a) 532 nm and b) 488 nm. The blue spectra are before illumination (dark), the red ones are light on, and the green ones correspond to the back-to-dark state.

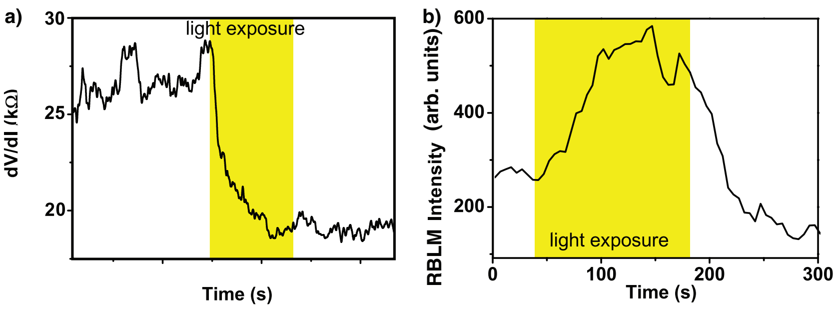


**Figure 4.** a) Differential resistance at $V_g$ = 22 V and b) RBLM peak intensity evolution under a cycle of white light on and off cycle.

the different enhancement factors between the Raman spectra at 532 and at 488 nm, only laser line at 488 nm exhibits a dramatic enhancement of optical phonons, while 532 nm line is resonant with the nanotube (RBLM are visible meaning the laser matches an electronic transition) but do not show so strong enhancement. These two observations strongly suggest that this enhancement arises from a resonance of the 488 nm line with the molecular charged state (after illumination) and with the excitonic state of the nanotube. Indeed, energy separation between the two laser lines (210 meV) is compatible with the energy of excitons in a nanotube.

Interestingly, the redox state reached by the molecule under light irradiation is stable for hours after illumination which accounts for the stable shift of the G mode whereas the non-conventional Raman effect disappears as the light is turned off. In order to get more insights into the underlying dynamics of these phenomena, we recorded the time evolution of the electrical and vibrational response of the hybrid device. **Figure 4** shows the resistance of a hybrid CNFET during a dark/light-on/light-off cycle as shown on the timeline. The gate voltage is set at a constant value of 22 V so that the CNFET is in the threshold regime and not fully saturated in order to gain electrostatic field sensitivity. When switching on the light, we observe a resistance decrease from 20 to 17 kΩ (−15%) which, according to the transfer characteristics shown in Figure 2, corresponds to an effective p-doping. The time needed to reach a new steady state is of about 100 s. When switching off the light after 80 s, we observe no significant change in the resistance of the device. We tested over 16 samples, among which only one went back to the previous state after 2 days in ambient conditions. However, by applying a gate voltage about −40 V on the backgate, we observe that within 150 s the resistance reaches a new steady state. In order to avoid the influence of the hysteresis, we then apply +30 V backgate voltage. When the backgate is tuned from 30 to 22 V, the resistance goes back to 22 kΩ, which is similar (−15%) to the dark state of the CNFET (not shown). Thus, we can use the backgate voltage to control and reset the illumination effect on the molecule in the hybrid in order to perform repeated operation of the optical switching of the device.

Similar behavior is observed in the vibrational response in burst mode Raman spectroscopy: a short accumulation time (1s) was used so as to record one spectrum every 5 s, and cycles of 100 s illumination followed by off states of 100 s were applied. For the first cycle, there is a clear doubling of the RBLM intensity (×2) when switching the light on, with a constant time of about 50 s, followed at the switching off by a decrease to a lower value than finally to the dark state (−25%) with a constant time of about 60 s. Almost the same behavior is observed on the G band (a lowering of −22% with a time constant around 40 s, not shown). Similar measurements were performed for non functionalized devices which showed no effect at all.

Both Raman and transport measurements show that two different dynamics come into play. First, a relatively fast process with a constant time of 50 s reveals the weak capacitive coupling between the nanotube and the molecules. The second process involves long characteristics time constants up to hours corresponding to the relaxation time of charges trapped around the nanotube either in the substrate or in molecules around.

From room temperature experiments we conclude that the dramatic enhancement of the phonon signature of the hybrid is due to the possibility of resonantly transferred excitons from the charged state of porphyrins to the nanotube under light exposure. Furthermore, the persistence of the light induced doping is strongly dependent on charge trapping in the nanotube vicinity. Charge trapping in nanotube transistors is related to adsorbates, defects or trapping sites in the oxide layer or at interfaces and is known to strongly modify effective doping.[31–34] Charge trapping is thermally activated, in order to get insights into trapping mechanisms, we record single charge trapping/detrapping in the nanotube vicinity at low temperature depending on the light irradiation.

When reaching low temperature (10 K), the transfer characteristics is similar to that observed at room temperature but exhibits additional features superimposed on the regular field effect response. These features are hysteretic conductance steps regularly spaced both in gate voltage and in the logarithm of the conductivity (**Figure 5**a). This behavior is assigned to single charge transfer between a trap and the nanotube as already observed in single electron memories[18] and CNFETs decorated with nanoparticles.[3,6] In the hybrid system, single charge tunneling occurs at low temperature between a molecular cluster and the nanotube, the latter being also a single charge electrometer. Considering the nanometer range of the nanotube diameter, electric field lines are concentrated at the nanotube surface, which promote charge tunneling with the environment and detection through field effect of the transistor. Such features are not observed on non functionalized nanotubes and are assigned to the presence of the deposited molecules. From the voltage change between two steps $\Delta V_g$, one can infer the capacitance $C_T$ between the trap T and the nanotube channel as

$$C_T = \frac{e}{\Delta V_g} \tag{1}$$

where $\Delta V_g$ = 0.56 V which gives $C_T$ = 0.3 aF. AFM performed on our devices shows that the molecular grains are larger than the nanotube diameter and about 30 nm (Supporting Information), so we can approximate $C_T$ with a simple cylinder-plane capacitance model

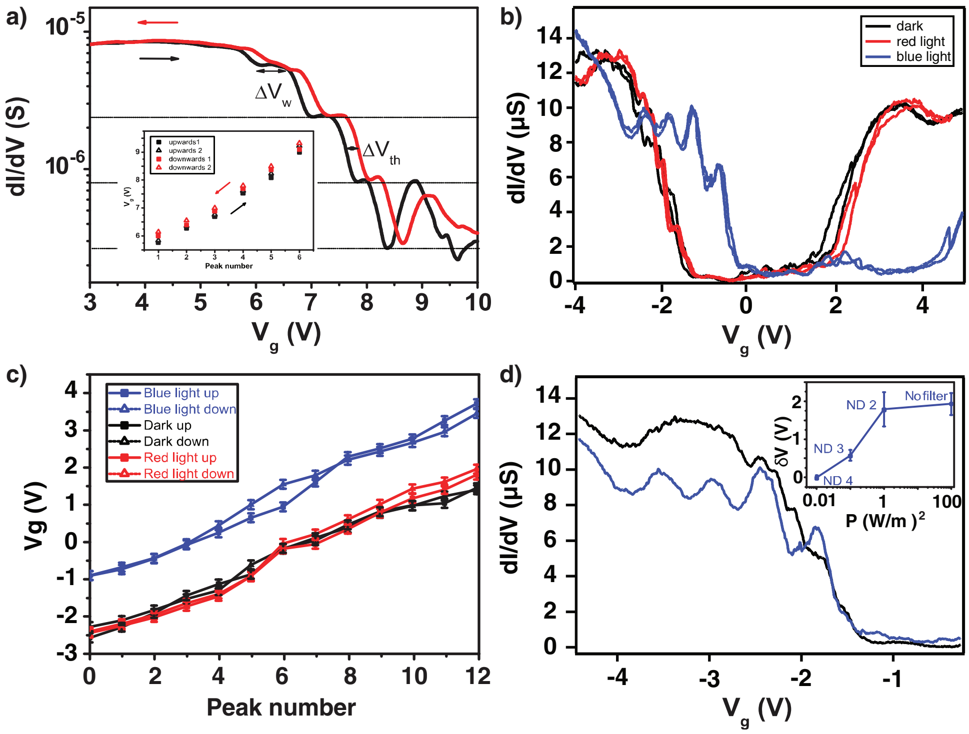


**Figure 5.** a) Low temperature transfer characteristics of DWNT/TPPZn hybrid transistor at 10 K. The curve is plotted at $V_{ds}$ = 1 mV (AC) for opposite gate sweeps of ±0.1 V $s^{-1}$ (inset shows the position of each step). b) Full hysteresis cycle of transfer characteristics of a DWNT/TPPZn hybrid transistor measured in dark (black curve), under red light illumination (red curve) and blue light (blue curve) at $V_{ds}$ = 1 mV (AC). c) Gate voltage position of the steps shown in (b). d) Same curves in dark and blue light for decreasing gate sweep and horizontally shifted for the sake of clarity (inset: light power dependence of the observed gate shift obtained using neutral densities).

$$C_T = \frac{2\pi d_T \varepsilon_0 \varepsilon_r}{\ln\left(\dfrac{h+\sqrt{h^2-d_{NT}^2}}{d_{NT}}\right)} \tag{2}$$

where $d_{NT}$ is the nanotube diameter (2 nm), $d_T$ is the trap size, and $h$ is the tunneling distance between the trap and the nanotube. We then obtain a distance of about 30 nm which allows to observe signatures of charge tunneling. Since the steps are regularly spaced in gate voltage, we conclude that the associated trap is not a single molecule which would rather exhibit molecular orbital spectrum. We thus attribute these regular peaks to a cluster of molecules in the Coulomb blockade regime. Furthermore, the presence of hysteresis between the up and down ramps of gate voltage is a signature of irreversibility in the charge tunneling (Figure 5a). Such irreversibility cannot occur in a single tunneling junction, but requires junctions in series implementing a so-called multiple tunneling junction (MTJ).[18] In such junctions, charges tunnel one by one along a series of potential wells which could be due in our case to tunneling from one molecule to another within the cluster before tunneling to the nanotube.

When exposing the device to light illumination, the power is low on the sample to prevent heating. For red light illumination (Figure 5b), we observe very little changes on the transfer characteristics: steps are still visible with the same spacing and shifted by only 0.1 V. Neither smoothing nor resistance change are visible which discards any eventual heating from light. Dramatic changes occur when using a blue filter including the absorption range of the molecule. First, we observe a global shift of the transfer characteristics by +1.5 V corresponding to an effective p-doping similar to the room temperature case. Moreover, we still detect quantized features which are regularly spaced with the same gate steps as without light, meaning that the trap self capacitance is still the same as without light. We attribute these features to the single charge transfers from the same molecular trap observed without light. This result is similar to what has been observed in porphyrins embedded in silica:[35] optical switching of tunneling effect was performed in molecule-based tunneling junctions. However this group observed a similar global shift at any wavelength which discarded the absorption by the molecules. In our case, the occurrence of a global shift for a wavelength matching the absorption peak of the molecule shows that the molecular optical transition is involved in the optical switching process. Furthermore, the most intriguing modification we observe is the shape of these features which, from a staircase-like in darkness, turn to sharp peaks under blue illumination. If heating was involved, such features would have turned even less sharp. This is then associated with a modification of the hysteresis in the trapping–detrapping event: when extracting the hysteresis area for the first step, we obtain an area $A_{dark} = 3.4 \times 10^{-6}$ S.V while under light exposure $A_{blue} = 1.6 \times 10^{-6}$ S.V which corresponds to a reduction of the hysteresis of 53%. According to Nakazato et al.,[18] this area is a function of the trap charging energy, the temperature and the ratio $\nu_s/\nu_{s0}$ where $\nu_s$ is the gate voltage sweep rate and $\nu_{s0} = (e/\tau)\ C_T$ is characteristic of MTJ and provides a time constant $\tau$ related to the charge tunneling dynamics. In our experiment, temperature and gate sweep rate are kept constant. We observe an overall shift of the characteristics upon blue light but the quantized steps exhibit same spacing as in the dark state. This spacing is directly proportional to the charging energy which we conclude to be constant upon illumination. From Nakazato's model, we conclude that the hysteresis area change is then directly due to a modification of the time constant $\tau$, pointing out to a modification in the dynamics of charge transfer through the MTJ, which is consistent with the work of Holloway et al.[36] Upon light exposure, the molecules involved in the MTJ turn excited which modifies the potential profile of the multiple barriers involved in the charge transfer to the nanotube. Indeed, Gruneis et al. have observed sharp features in the case of a trap being very well coupled to a nanotube.[6] In our case, we conclude that from a weak nanotube–trap coupling in darkness, light allows optical switching of the MTJ into a strong coupling regime. The change in the coupling is difficult to quantify since we do not have information about the structure of the MTJ. Still since the hysteresis area is divided only by a factor two, we can conclude that the coupling is moderately tuned by light. This modification is though sufficient to observe modification of quantized steps into peaks related to the change of dynamics.

In summary, we demonstrate in this work the possibility to get a light-activated transistor based on a chromophore-coated single nanotube hybrids acting down to the single charge transfer limit at low temperature. We have shown that beyond charge transfer, photogating of hybrid nanotube/chromophore goes along with an unusual Raman signal enhancement for laser excitation energies which match the chromophore absorption range. This photogenerated Raman enhancement is a consequence of the energy transfer between the charged state of the molecule (after light absorption) and the excitonic state of the nanotube which leads to a renormalization of the Raman cross section. Both transport and Raman signals exhibit such spectral dependence.

Moreover, at low temperature, light exposure induces optical switching of the charge tunneling with a spectral dependence related to the molecule absorption spectrum. Furthermore, we also demonstrate the light action on kinetics in the carbon-nanotube-based single electron memories. The control of single charge tunneling with light is a novel aspect that will be further exploited with a better control of the chromophore nanotube coating.

## Experimental Section

*Fabrication of the Devices*: A powder of catalytic-Chemical Vapor Deposition double wall carbon nanotubes[37] was dispersed by ultrasonics in 1,2-dichloroethane by mild sonication. About 20 µL of the suspension was deposited onto a patterned $SiO_2$/Si wafer by spin-coating. After deposition, DWNTs were located by low voltage scanning electron microscopy (SEM) to design 50 nm thick Pd electrodes by e-beam lithography. The lengths of the DWNTs were between 1 and 2 µm.

*Characterization of the Hybrids*: Absorption spectra were recorded using a VIS/NIR Lambda 900 spectrometer. Raman measurements were performed by using a confocal Witec alpha 500 and a T64000 Jobin Yvon spectrometer. In Witec spectrometer, the elastically scattered light from the sample was filtered out by a Notch filter, while the inelastically scattered light was collected and sent to a spectrometer with a resolution less than 1 $cm^{-1}$. A typical Raman spectrum was acquired in 1–10 s. To avoid laser heating, laser power was kept below 0,5 mW $\mu m^{-2}$. Regarding the Raman spectra at 488 nm, the inelastic light was measured in the back-scattering configuration on a triple substractive Jobin Yvon T64000 micro-spectrometer in the same experimental conditions as on the Witec spectrometer. Room temperature transistor characteristics were obtained with a vacuum Desert Cryogenics probe station using two beryllium-copper probes. Transfer characteristics ($I_{ds}$, $V_g$) curves were acquired in a current-biased lock-in configuration using a Stanford Research 830 lock-in amplifier. The transistor characteristics of the device were measured by applying a 50 nA drain–source current while sweeping the gate voltage between ±30 V. Light illumination of the device was performed by using X-Cite 120Q excitation white light source with a constant power about 100 W and different color filters (see Supporting Information). The low temperature transport measurements were performed in a Janis optical cryostat down to 10 K.

## Supporting Information

Supporting Information is available from the Wiley Online Library or from the author.

## Acknowledgements

L.M. and N.B. contributed equally to this work. The authors wish to thank B. Soula, E. Anglaret, V. Jourdain, M. Holzinger, and R. Martel for fruitful discussions, and V. Reita, D. Jegouso, and T. Crozes for technical support. This work was supported by TRICO ANR, LANEF program (Cryoptics), and the Chinese Scholarship Council.

[1] J.-C. Charlier, S. Roche, *Rev. Mod. Phys.* **2007**, *79*, 677.
[2] P. Avouris, M. Freitag, V. Perebeinos, *Nat. Photonics* **2008**, *2*, 341.
[3] L. Marty, A.-M. Bonnot, A. Bonhomme, A. Iaia, C. Naud, E. André, V. Bouchiat, *Small* **2006**, *2*, 110.
[4] A. T. C. Johnson, C. Staii, M. Chen, S. Khamis, R. Johnson, M. L. Klein, A. Gelperin, *Phys. Status Solidi B* **2006**, *243*, 3252.
[5] J. Borghetti, V. Derycke, S. Lenfant, P. Chenevier, A. Filoramo, M. Goffman, D. Vuillaume, J.-P. Bourgoin, *Adv. Mater.* **2006**, *18*, 2535.
[6] A. Gruneis, M. J. Esplandiu, D. Garcia-Sanchez, A. Bachtold, *Nano Lett.* **2007**, *7*, 3766.
[7] L. Bogani, C. Danieli, E. Biavardi, N. Bendiab, A.-L. Barra, E. Dalcanale, W. Wernsdorfer, A. Cornia, *Angew. Chem.* **2009**, *48*, 746.
[8] M. Urdampilleta, S. Klyatskaya, J.-P. Cleuziou, M. Ruben, W. Wernsdorfer, *Nat. Mater.* **2011**, *10*, 502.
[9] D. Bouilly, J. Cabana, F. Meunier, M. Desjardins-Carrière, F. Lapointe, P. Gagnon, F. L. Larouche, E. Adam, M. Paillet, R. Martel, *ACS Nano* **2011**, *5*, 4927.
[10] M. Ganzhorn, S. Klyatskaya, M. Ruben, W. Wernsdorfer, *Nat. Nanotechnol.* **2013**, *8*, 165.
[11] D. S. Hecht, R. J. Ramirez, M. Briman, E. Artukovic, K. S. Chichak, J. F. Stoddart, G. Grüner, *Nano Lett.* **2006**, *6*, 2031.

[12] A. Yella, H.-W. Lee, H. N. Tsao, C. Yi, A. K. Chandiran, M. K. Nazeeruddin, E. W.-G. Diau, C.-Y. Yeh, S. M. Zakeeruddin, M. Grätzel, *Science* **2011**, *334*, 629.
[13] R. Chitta, A. S. Sandanayaka, A. L. Schumacher, L. D'Souza, Y. Araki, O. Ito, F. D'Souza, *J. Phys. Chem. C* **2007**, *111*, 6947.
[14] C. Roquelet, D. Garrot, J.-S. Lauret, C. Voisin, V. Alain-Rizzo, P. Roussignol, J. Delaire, E. Deleporte, *Appl. Phys. Lett.* **2010**, *97*, 141918.
[15] A. Satake, Y. Miyajima, Y. Kobuke, *Chem. Mater.* **2005**, *17*, 716.
[16] X. Ling, L. Xie, Y. Fang, H. Xu, H. Zhang, J. Kong, M.-S. Dresselhaus, J. Zhang, Z. Liu, *Nano Lett.* **2010**, *10*, 553.
[17] S. Huang, X. Ling, L. Liang, Y. Song, W. Fang, J. Zhang, J. Kong, V. Meunier, M.-S. Dresselhaus, *Nano Lett.* **2015**, *15*, 2892.
[18] K. Nakazato, R. J. Blaikie, H. Ahmed, *J. Appl. Phys.* **1994**, *75*, 5123.
[19] D. Wöhrle, G. Schnurpfeil, *Porphyrin Handb.* **2003**, *11*, 177.
[20] G. Magadur, J.-S. Lauret, G. Charron, F. Bouanis, E. Norman, V. Huc, C.-S. Cojocaru, S. Gómez-Coca, E. Ruiz, T. Mallah, *J. Am. Chem. Soc.* **2012**, *134*, 7896.
[21] K. S. Suslick, N. A. Rakow, M. E. Kosal, J. H. Chou, *J. Porphyrins Phtalocyanines* **2000**, *4*, 407.
[22] J. Correa, W. Orellana, *Phys. Rev. B* **2012**, *86*, 125417.
[23] F. Vialla, C. Roquelet, B. Langlois, G. Delport, S. M. Santos, E. Deleporte, P. Roussignol, C. Delalande, C. Voisin, J.-S. Lauret, *Phys. Rev. Lett.* **2013**, *111*, 137402.
[24] C. B. Winkelmann, I. Ionica, X. Chevalier, G. Royal, C. Bucher, V. Bouchiat, *Nano Lett.* **2007**, *7*, 1454.
[25] D. H. Jeong, M.-C. Yoon, S. M. Jang, D. Kim, D. W. Cho, N. Yoshida, N. Aratani, A. Osuka, *J. Phys. Chem. A* **2002**, *106*, 2359.
[26] M. Lopes, A. Candini, M. Urdampilleta, A. Reserbat-Plantey, V. Bellini, S. Klyatskaya, L. Marty, M. Ruben, M. Affronte, W. Wernsdorfer, N. Bendiab, *ACS Nano* **2010**, *4*, 7531.
[27] D. M. Andrada, H. S. Vieira, M. M. Oliveira, A. P. Santos, L. Yin, R. Saito, M. A. Pimenta, C. Fantini, C. A. Furtado, *Carbon* **2013**, *56*, 235.
[28] A. Das, S. Pisana, B. Chakraborty, S. Piscanec, S. K. Saha, U. V. Waghmare, K. S. Novoselov, H. R. Krishnamurthy, A. K. Geim, A. C. Ferrari, A. K. Sood, *Nat. Nanotechnol.* **2008**, *3*, 210.
[29] F. Vialla, E. Malic, B. Langlois, Y. Chassagneux, C. Diederichs, E. Deleporte, P. Roussignol, J.-S. Lauret, C. Voisin, *Phys. Rev. B* **2014**, *90*, 155401.
[30] S. K. Islam, M. A. Sohel, J. R. Lombardi, *J. Phys. Chem. C* **2014**, *118*, 19415.
[31] M. Radosavljević, M. Freitag, K. V. Thadani, A. T. Johnson, *Nano Lett.* **2002**, *2*, 761.
[32] M. S. Fuhrer, B. M. Kim, T. Dürkop, T. Brintlinger, *Nano Lett.* **2002**, *2*, 755.
[33] W. B. Choi, S. Chae, E. Bae, J.-W. Lee, B.-H. Cheong, J.-R. Kim, J.-J. Kim, *Appl. Phys. Lett.* **2003**, *82*, 275.
[34] C. M. Aguirre, P. L. Levesque, M. Paillet, F. Lapointe, B. C. St-Antoine, P. Desjardins, R. Martel, *Adv. Mater.* **2009**, *21*, 3087.
[35] Y. Wakayama, K. Ogawa, T. Kubota, H. Suzuki, T. Kamikado, S. Mashiko, *Appl. Phys. Lett.* **2004**, *85*, 329.
[36] G. W. Holloway, Y. Song, C. M. Haapamaki, R. R. LaPierre, J. Baugh, *J. Appl. Phys.* **2013**, *113*, 024511.
[37] E. Flahaut, R. Bacsa, A. Peigney, C. Laurent, *Chem. Commun.* **2003**, 12, 1442.

# Supporting Information

for *Adv. Mater.,* DOI: 10.1002/adma.201605745

## Light Control of Charge Transfer and Excitonic Transitions in a Carbon Nanotube/Porphyrin Hybrid

*Yani Chen, Guy Royal, Emmanuel Flahaut, Saioa Cobo, Vincent Bouchiat, Laëtitia Marty, and Nedjma Bendiab**

# Supplementary information: Light control of charge transfer and excitonic transitions in a carbon nanotube/porphyrin hybrid

Yani Chen,[†] Guy Royal,[‡] Emmanuel Flahaut,[¶] Saioa Cobo,[‡] Vincent Bouchiat,[†] Laëtitia Marty,[†] and Nedjma Bendiab[*,†]

*†Institut Néel, Université Grenoble Alpes, BP 166, Grenoble Cedex 9, 38042, France*

*‡Univ. Grenoble Alpes, DCM UMR 5250, F-38000 Grenoble, France; CNRS, DCM UMR 5250, F-38000 Grenoble, France*

*¶CIRIMAT, UMR CNRS-UPS-INP N°5085, Université Toulouse 3 Paul Sabatier, Bât. CIRIMAT, 118, route de Narbonne, 31062 Toulouse cedex 9, France*

E-mail: nedjma.bendiab@neel.cnrs.fr

**Characterization of DWNTs** Figure 1a) shows the Raman spectra of many bundles from the DWNT powder before dispersion (red line) measured using a 532 nm excitation wavelength. The multiple RBLM peaks in the DWNT spectrum indicate the presence of different diameters in the DWNT bundles. Typical RBLM signature of DWNTs are observed. The first RBLM group contains two main peaks at 159 $cm^{-1}$ and 191 $cm^{-1}$, whereas for the second group, the two main peaks are observed at 270 $\mathrm{cm}^{-1}$ and 320 $\mathrm{cm}^{-1}$. Thus, the corresponding two most often observed outer wall diameters are around 1.53 nm and 1.22 nm, whereas the two main inner wall diameters are 0.89 nm and 0.73 nm.[1]

For the bare DWNT transistor (black line), two peaks can be observed in the RBLM range. We assign the peak at 302 $\mathrm{cm}^{-1}$ to the silicon substrate, and the peak at 273 $\mathrm{cm}^{-1}$ to a RBLM peak from the DWNT transistor. We estimate the inner diameter of this excited nanotube to be around 0.9 nm. By comparison to the associated DWNT bundles, this isolated DWNT is a semiconducting tube regarding its RBLM and G mode in comparaison to the Kataura plot. Since the full width at half maximum (FWHM) of this RBLM is only 4.7 $cm^{-1}$ (close to the instrumental function FWHM), we can claim its isolated character. Usually, the linewidths obtained from the DWNT bundles are larger (from 11 to 27 $cm^{-1}$). Since the smallest RBLM linewidth values (the natural linewidths) occur under the strongest resonance conditions where $E_{laser} - E_{ii} = 0$ , for both isolated metallic and semiconducting SWNTs[2] , such a small linewidth indicates that this sample meets the strong resonance requirement at 532 nm. Moreover, in the G peak region, a metallic like BWF shoulder appears indicating the presence of a metallic tube in this DWNT transistor, which can only be the outer tube. Therefore, this tube has a S @ M configuration.

Figure 1b) is the transfer characteristics of typical metallic and semiconducting double wall carbon nanotubes. We can compare the transfer characteristics to the Raman spectra in order to get more information. The DWNTs have four kinds of metallic and semiconducting configurations, which are M@M, M@S, S@M, S@S tubes. Theoretically, the proportion of these four kinds of tubes are $\frac{1}{9}$, $\frac{2}{9}$, $\frac{2}{9}$ and $\frac{4}{9}$, respectively (experimentally, it is not straightforward to observe similar probabilities[3]). Figure 1c) shows the statistics of on/off current ratio ($I_{on}/I_{off}$) of 25 pristine isolated DWNT FETs, among which, we find that 3 tubes have $I_{on}/I_{off}$ =1, which means these 3 tubes have M@M configuration. Similarly, for the $I_{on}/I_{off} > 30$, there are 8 tubes, the proportion of which satisfies the distribution of S@S tubes. The $I_{on}/I_{off}$ of the rest of tubes are between 1 and 5, which may have M@S or S@M configuration. From Figure 1 c), we can observe that the distribution correlates quite well with the theory, therefore, we can roughly estimate that in our experiment, if $I_{on}/I_{off} > 30$, the DWNT has S@S configuration; if $1 < I_{on}/I_{off} <30$, the DWNT is a M@S or S@M tube; if $I_{on}/I_{off} = 1$, then the DWNT is a M@M tube. As shown in Figure 2b), $I_{on}/I_{off}$ of this pristine DWNT is around 8, therefore, this DWNT is M@S or S@M tube. This result is in agreement with the Raman spectra discussed above.

**Molecule interaction with DWNT** In the main text, we discussed the Raman spectra of the isolated DWNTs before and after grafting TPPZn. Since BWF line shape is observed, the G peak region was fitted with 3 Lorentzian peaks and one Fano-like peak. The fitting parameters are shown in Table 1.

The Raman spectra show several evidences for charge transfer between nanotube and molecules:

1. Shift of G peak: the pristine spectrum shows four peaks, the two highest are assigned to $G^+$ components of each two walls and the two lowest to the $G^-$ ones. After doping with TPPZn, $\omega_{G1}$ shifts from 1591.6 to 1589.2 $cm^{-1}$ ( $\delta = -2.4cm^{-1}$ ), $\omega_{G2}$ shifts from 1574.2 to 1571.8 $cm^{-1}$ ( $\delta = -2.4cm^{-1}$ ). Comparing with the G mode shift for molecule-induced doping of SWNTs[4,5] and graphene,[6] we infer that the outer wall was n-doped, because the G peaks downshift. The intensity of $G^+$ peak increased after the deposition of TPPZn. The intensity ratio $IG^+_{pristine}$ / $IG^+_{hybrid}$ is 19.5. Such large increase of the intensity originates from chemical enhancement induced by TPPZn. The charge transfer between TPPZn and the DWNT, induces a Fermi level shift. To roughly estimate this shift, we compare the G peak shift to the electrostatically induced doping[7–10] which allows us to estimate a modification of the Fermi energy about 20 meV to 43 meV. Moreover, from probe test measurement, and by using the equation

$$\Delta E_F = \frac{\hbar}{2} V_F \Delta n \tag{1}$$

we calculate an increase of charge carrier density, $\Delta n$ about 60 to 130 e$^-$ /$\mu$m. Furthermore, other theoretical and experimental work also claim that the interaction of CNT with porphyrin leads to red shifts in the optical transition of less than 10 meV.[11,12]

2. Figure 2 a) and b) show the Lorentzian fitting of the Raman 2D peak of pristine

DWNT and DWNT/TPPZn transistor. Each curve can be fitted into two peaks, which originate from the two walls of the DWNT.[13] We can observe that the intensity ratio of the first to the second peak $I_{2D1}/I_{2D2}$ increases a little, from 2.5 to 6.5, which also points out the chemical enhancement phenomenon.

Finally, figure 3 b) shows the transfer characteristics curves of isolated DWNT (black) and DWNT/TPPZn hybrid (blue) FETs. The bare DWNT FET exhibits p-type field effect characteristics from doping with air exposure. After porphyrin coating, the DWNT exhibits a conductance drop of 80%, which could be the result of the addition of charge scattering sites distributed randomly along the nanotube.[14] The second change is an increase of the on to off ratio from 7 to 65, which may be attributed to the fact that porphyrins reduce conduction along the metallic outer wall which reveals the semiconducting behaviour of the inner one. We also observe that the addition of porphyrins introduces a 4.5 V shift in the threshold voltage towards negative gate voltage. The direction of the shift is in agreement with the results of Hecht *et al.*:[14] in SWNT hybrid devices, changes in threshold voltage are attributed to charge transfer of the functionalized donor to the acceptor molecule.[15,16] The electron-donating molecule leads to a shift towards negative gate voltages. Concerning the charge traps observed at low temperature on hybrid devices, Figure 2 a) shows the equivalent circuit of the nanotube-porphyrin hybrid used in the main text to calculate the charge trap size. Figure 2 c) shows the spectra of the sources used to excite the hybrid FET at low temperature. AFM microscopy of a functionalized device (Figure 2 d)) reveals the presence of clusters along the nanotube which are not present before molecular deposition. The size of these clusters corresponds to the expected size of the charge traps (few nm up to 40nm). Thus, from the cross comparison of electron transport and vibrational characteristics, we can conclude that deposited TPPZn transfer 60 to 130 charges per micron to the connected DWNT, the DWNT Fermi level shift is around 20 to 43 meV.

Table 1: Peak fit summary for the spectra measured at 532 nm.

| | DWNT | DWNT/TPPZn dark | DWNT/TPPZn light on | DWNT/TPPZn light off |
|---|---|---|---|---|
| $\omega_{G1}$ (cm$^{-1}$) | 1591.6 | 1589.2 | 1589.8 | 1589.5 |
| $\Gamma_{G1}$ (cm$^{-1}$) | 6.4 | 9.0 | 8.9 | 8.7 |
| $\omega_{G2}$ (cm$^{-1}$) | 1580.9 | 1582.0 | 1580.1 | 1580.2 |
| $\Gamma_{G2}$ (cm$^{-1}$) | 4.2 | 4.4 | 3.1 | 3.8 |
| $\omega_{G3}$ (cm$^{-1}$) | 1574.2 | 1571.8 | 1571.9 | 1571.1 |
| $\Gamma_{G3}$ (cm$^{-1}$) | 9.0 | 8.0 | 8.0 | 10.6 |
| $\omega_{Fano}$ (cm$^{-1}$) | 1527.6 | 1521.5 | 1515.8 | 1513.2 |
| $\Gamma_{Fano}$ (cm$^{-1}$) | 99.3 | 106.1 | 64.2 | 81.7 |
| Q | -2.3 | -3.9 | -3.8 | -5.4 |
| $\omega_{RRBLM}$ (cm$^{-1}$) | 273.1 | 273.8 | 274.0 | 274.0 |
| $\Gamma_{RRBLM}$ (cm$^{-1}$) | 4.7 | 3.2 | 3.9 | 3.9 |
| $I_{RRBLM}$ | 0.03 | 0.21 | 0.13 | 0.15 |
| $I_{G1}$ | 0.035 | 0.20 | 0.10 | 0.13 |
| $\omega_{2D1}$ (cm$^{-1}$) | 2628.9 | 2624.8 | 2621.7 | 2622.2 |
| $\Gamma_{2D1}$ (cm$^{-1}$) | 43.5 | 31.7 | 32.2 | 32.2 |
| $\omega_{2D2}$ (cm$^{-1}$) | 2681.1 | 2672.1 | 2668.9 | 2669.2 |
| $\Gamma_{2D2}$ (cm$^{-1}$) | 45.2 | 28.3 | 36.7 | 31.7 |

# References


(1) Cambedouzou, J.; Sauvajol, J.-L.; Rahmani, A.; Flahaut, E.; Peigney, A.; Laurent, C. *Phys. Rev. B* **2004**, *69*, 235422.

(2) Jorio, A.; Pimenta, M.; Souza Filho, A.; Saito, R.; Dresselhaus, G.; Dresselhaus, M. *New Journal of Physics* **2003**, *5*, 139.

(3) Ghedjatti, A. Etude structurale des nanotubes de carbone double parois par microscopie électronique en transmission haute résolution et absorption optique. Ph.D. thesis, Paris VI, 2016.

(4) Rao, A. M.; Eklund, P.; Bandow, S.; Thess, A.; Smalley, R. E. *Nature* **1997**, *388*, 257–259.

(5) Shim, M.; Ozel, T.; Gaur, A.; Wang, C. *Journal of the American Chemical Society* **2006**, *128*, 7522–7530.

(6) Lopes, M.; Candini, A.; Urdampilleta, M.; Reserbat-Plantey, A.; Bellini, V.; Klyatskaya, S.; Marty, L.; Ruben, M.; Affronte, M.; Wernsdorfer, W.; Bendiab, N. *ACS Nano* **2010**, *4*, 7531–7537.

(7) Stampfer, C.; Molitor, F.; Graf, D.; Ensslin, K.; Jungen, A.; Hierold, C.; Wirtz, L. *Applied Physics Letters* **2007**, *91*.

(8) Yan, J.; Zhang, Y.; Kim, P.; Pinczuk, A. *Physical Review Letters* **2007**, *98*.

(9) Das, A.; Pisana, S.; Chakraborty, B.; Piscanec, S.; Saha, S. K.; Waghmare, U. V.; Novoselov, K. S.; Krishnamurthy, H. R.; Geim, A. K.; Ferrari, A. C.; Sood, A. K. *Nature Nanotechnology* **2008**, *3*, 210–5.

(10) Farhat, H.; Son, H.; Samsonidze, G. G.; Reich, S.; Dresselhaus, M. S.; Kong, J. *Phys. Rev. Lett.* **2007**, *99*, 145506.

(11) Roquelet, C.; Garrot, D.; Lauret, J.-S.; Voisin, C.; Alain-Rizzo, V.; Roussignol, P.; Delaire, J.; Deleporte, E. *Applied Physics Letters* **2010**, *97*, 141918.

(12) Correa, J.; Orellana, W. *Physical Review B* **2012**, *86*, 125417.

(13) Villalpando-Paez, F.; Son, H.; Nezich, D.; Hsieh, Y. P.; Kong, J.; Kim, Y.; Shimamoto, D.; Muramatsu, H.; Hayashi, T.; Endo, M.; Terrones, M.; Dresselhaus, M. S. *Nano Letters* **2008**, *8*, 3879–3886.

(14) Hecht, D. S.; Ramirez, R. J.; Briman, M.; Artukovic, E.; Chichak, K. S.; Stoddart, J. F.; Grüner, G. *Nano Letters* **2006**, *6*, 2031–2036.

(15) Bradley, K.; Gabriel, J.-C. P.; Briman, M.; Star, A.; Grüner, G. *Physical Review Letters* **2003**, *91*, 218301.

(16) Hu, L.; Zhao, Y. L.; Ryu, K.; Zhou, C.; Stoddart, J. F.; Grüner, G. *Advanced Materials* **2008**, *20*, 939–946.

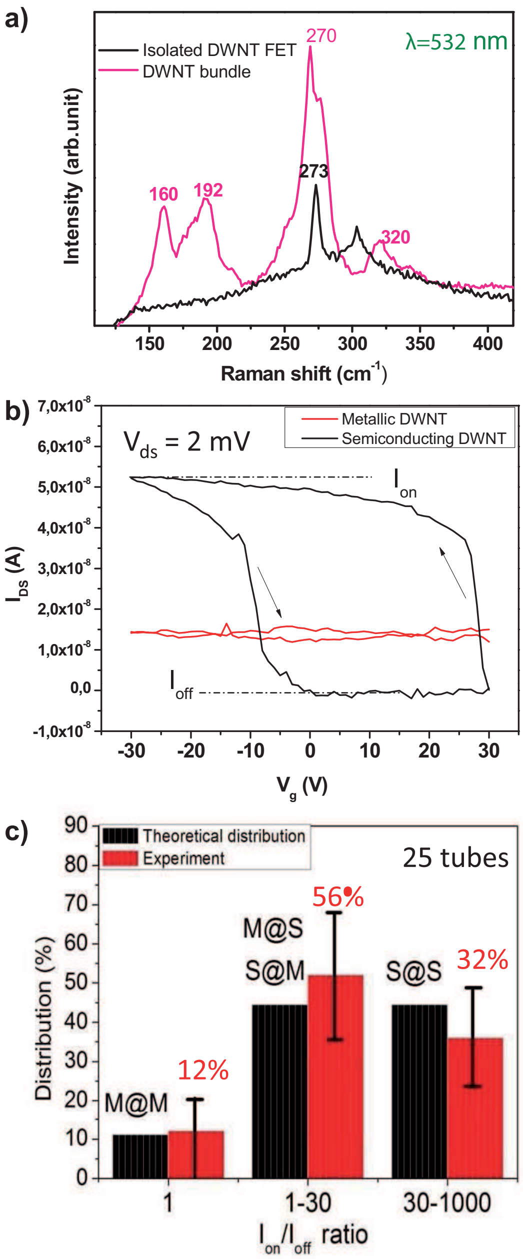


Figure 1: a) Raman spectra of DWNT bundles and isolated DWNT transistor at 532 nm; b) Typical transfer characteristic curves of individual metallic and semiconducting DWNT; c) Distribution of the on/off current ratio for the pristine isolated DWNT FETs.

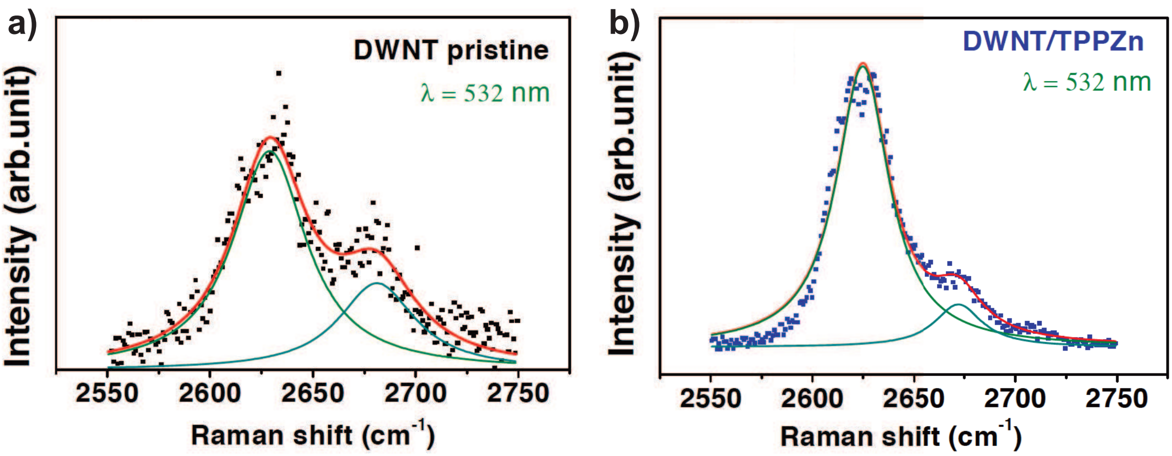


Figure 2: Typical 2D peaks of pristine DWNT before (a) and after (b) TPPZn deposition.

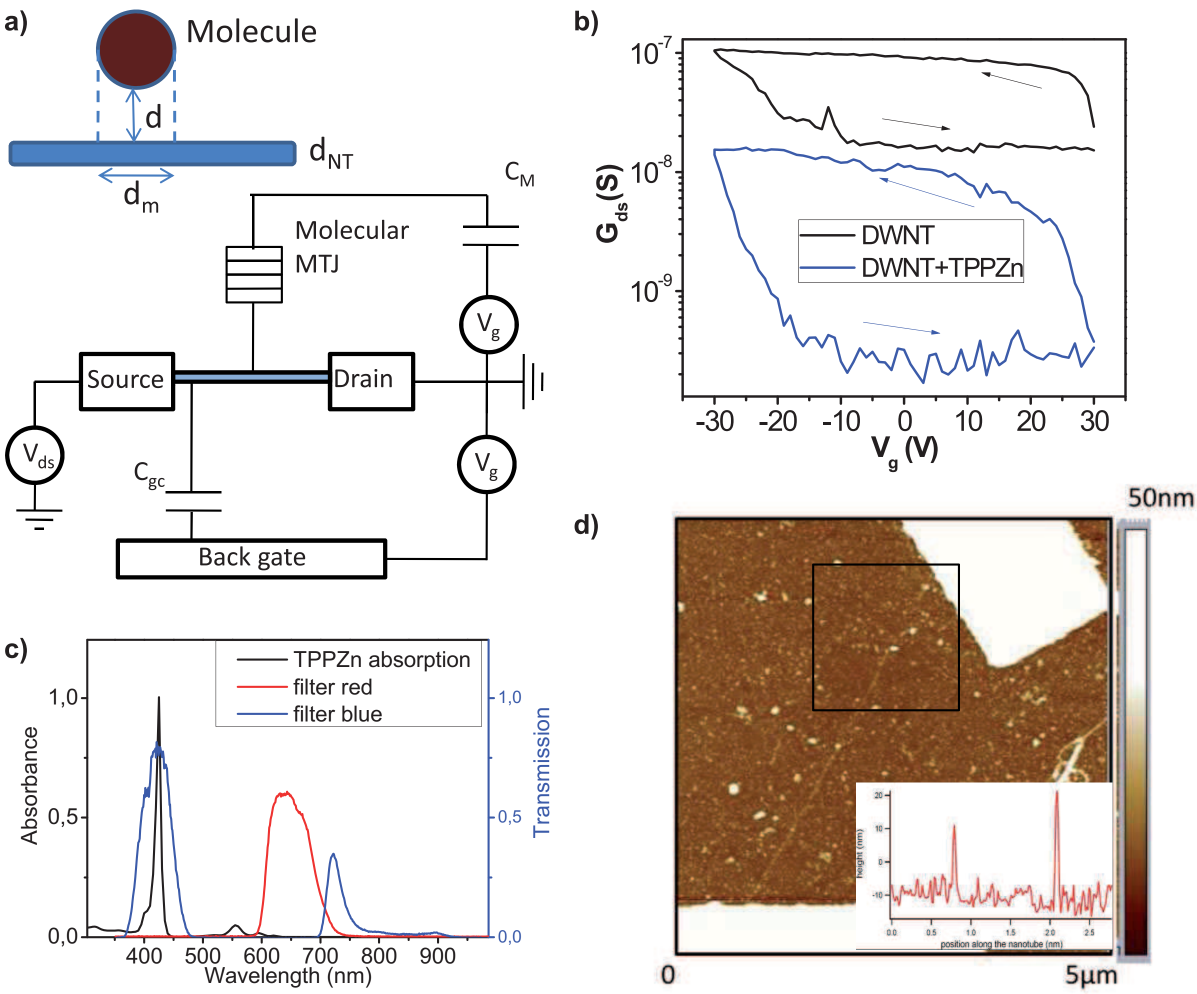


Figure 3: a) Capacitive model of the hybrid FET at low temperature; b) Transfer characteristic curves for DWFET before (black) and after (blue) TPPZn deposition, c) Transmission spectra of red and blue filter and absorption spectrum of TPPZn; d) AFM image of an isolated DWNT transistor after TPPZn deposition (inset of is the cut along the DWNT which shows distribution of clusters from few nm up to 40 nm).